

Hemodialysis arterio-venous graft design reducing the hemodynamic risk of vascular access dysfunction

*Original*

Hemodialysis arterio-venous graft design reducing the hemodynamic risk of vascular access dysfunction / De Nisco, Giuseppe; Gallo, Diego; Siciliano, Katia; Tasso, Paola; Lodi Rizzini, Maurizio; Mazzi, Valentina; Calò, Karol; Antonucci, Marta; Morbiducci, Umberto. - In: JOURNAL OF BIOMECHANICS. - ISSN 0021-9290. - STAMPA. - 100:(2020), pp. 1-11. [10.1016/j.jbiomech.2019.109591]

*Availability:*

This version is available at: 11583/2786276 since: 2020-02-24T14:51:35Z

*Publisher:*

Elsevier

*Published*

DOI:10.1016/j.jbiomech.2019.109591

*Terms of use:*

This article is made available under terms and conditions as specified in the corresponding bibliographic description in the repository

*Publisher copyright*

Elsevier postprint/Author's Accepted Manuscript

© 2020. This manuscript version is made available under the CC-BY-NC-ND 4.0 license  
<http://creativecommons.org/licenses/by-nc-nd/4.0/>. The final authenticated version is available online at:  
<http://dx.doi.org/10.1016/j.jbiomech.2019.109591>

(Article begins on next page)

Title page

## **Hemodialysis Arterio-venous Graft Design Reducing the Hemodynamic Risk of Vascular Access Dysfunction**

Giuseppe De Nisco<sup>1</sup>, Diego Gallo<sup>1</sup>, Katia Siciliano<sup>1</sup>, Paola Tasso<sup>1</sup>, Maurizio Lodi Rizzini<sup>1</sup>, Valentina Mazzi<sup>1</sup>, Karol Calò<sup>1</sup>, Marta Antonucci<sup>2</sup>, Umberto Morbiducci<sup>1†</sup>

<sup>1</sup> *Polito<sup>BIO</sup>Med Lab, Department of Mechanical and Aerospace Engineering, Politecnico di Torino, Turin, Italy*

<sup>2</sup> *Cardiovascular Lab SpA, Milan, Italy*

***The final publication is available at [link.springer.com](http://link.springer.com)***

**†Address for correspondence:**

Umberto Morbiducci, Ph.D.

Department of Mechanical and Aerospace Engineering, Politecnico di Torino

Corso Duca degli Abruzzi, 24 - 10129 Turin, Italy

Tel.: +39 011 0906882

Fax: +39 011 5646999

E-mail: [umberto.morbiducci@polito.it](mailto:umberto.morbiducci@polito.it)

## Abstract and key terms

Although arterio-venous grafts (AVGs) represent the second choice as permanent vascular access for hemodialysis, this solution is still affected by a relevant failure rate due to graft thrombosis, and development of neointimal hyperplasia (IH) at the distal vein. As a key role in these processes has been attributed to the abnormal hemodynamics establishing in the distal vein, the optimization of AVGs design aimed at minimizing flow disturbances would reduce AVG hemodynamic-related risks. In this study we used computational fluid dynamics to investigate the impact of alternative AVG designs on the reduction of IH and thrombosis risk at the distal venous anastomosis. The performance of the newly designed AVGs was compared to that of commercially available devices. In detail, a total of eight AVG models in closed-loop configuration were constructed: two models resemble the commercially available straight conventional and helical-shaped AVGs; six models are characterized by the insertion of a flow divider (FD), straight or helical shaped, differently positioned inside the graft. Unfavorable hemodynamic conditions were analyzed by assessing the exposure to disturbed shear at the distal vein. Bulk flow was investigated in terms of helical blood flow features, potential thrombosis risk, and pressure drop over the graft.

Findings from this study clearly show that using a helically-shaped FD located at the venous side of the graft could induce beneficial helical flow patterns that, minimizing flow disturbances, reduce the IH-related risk of failure at the distal vein, with a clinically irrelevant increase in thrombosis risk and pressure drop over the graft.

**Keywords:** Vascular access; Arterio-venous graft; Helical flow; Computational fluid dynamics.

## Introduction

Patients with end stage renal disease depend on hemodialysis as primary form of kidney function replacement, and thus are in need of a permanent vascular access to ensure an effective treatment ([Ene-lordache and Remuzzi, 2017](#)). When arterio-venous fistula placement is not possible, arterio-venous graft (AVG) represents the second-best option ([Scott and Glickman, 2007](#); [Shiu et al., 2019](#)). Technically, in AVG-based hemodialysis, an artery and a vein are surgically connected *via* a synthetic graft, positioned in a closed-loop or straight configuration and superficially tunneled under the skin ([Ene-lordache and Remuzzi, 2017](#)).

Although clinical guidelines ([NKFK/DOQI, 2006](#); [Tordoir et al., 2007](#)) recommend well-defined criteria for AVG placement (in particular in patients with weak and/or small veins), a not negligible failure rate is still reported worldwide (cumulative graft failure higher than 50%, see [Dixon et al., 2009](#) and [Shiu et al., 2019](#)), thus affecting its clinical use ([Pisoni et al., 2015](#); [Sequeira et al., 2017](#)). In particular, AVG failure is markedly associated with thrombus formation in the graft and progressive neointimal hyperplasia (IH) that leads to the lumen obstruction ([Allon, 2007](#); [Ene-lordache and Remuzzi, 2017](#); [Hodges et al., 1997](#); [Kelly et al., 2002](#); [Li et al., 2008](#); [Roy-Chaudhury et al., 2001](#)).

Among the causes of IH onset and progression in hemodialysis vascular access, abnormal hemodynamics has been proposed as a primary promoter ([Loth et al., 2003](#)). This is supported by clinical observations on stenosis occurrence mainly at the AVG graft-venous anastomosis (around 80% of cases, [Kanterman et al., 1995](#)) or in the draining vein, where abnormal hemodynamics develops ([Allon, 2007](#); [Beathard, 2002](#); [Li et al., 2008](#); [Loth et al., 2003, 2008](#); [Maya et al., 2004](#); [Roy-Chaudhury et al., 2001, 2006](#)). A large body of literature further supports the hemodynamic risk of failure hypothesis for AVG ([Cunnane et al. 2017](#)), reporting that AVG placement might induce unphysiological hemodynamic conditions at the graft-venous side, exposing the venous

wall to deranged hemodynamics ([Bassiouny et al., 1992](#); [Caro et al., 1971](#); [Cunnane et al., 2017](#); [Ene-Iordache and Remuzzi, 2017](#); [Himburg et al., 2004](#); [Loth et al., 2003, 2008](#); [Ojha, 1993](#); [Rittgers et al., 1978](#); [Roy-Chaudhury et al., 2006, 2007](#); [Sherwin et al., 2000](#)).

Evidences of a hemodynamic risk of failure through IH has stimulated the hemodynamic optimization of AVG device design. In this context, the documented physiological significance of helical blood flow, with its beneficial role in suppressing flow disturbances ([Bogren and Bonocore, 1994](#); [De Nisco et al., 2019](#); [Gallo et al., 2012, 2015, 2018](#); [Liu et al., 2009, 2015](#); [Morbideucci et al., 2007, 2009, 2011, 2013](#); [Stonebridge et al., 1996](#)), has led to rethink AVGs also in terms of helical blood flow inducers, thus improving the performance of the device. In particular, [Caro et al. \(2005, 2007\)](#) first developed and tested helical-shaped grafts in a porcine model study, reporting consistently less thrombosis and IH than conventional grafts ([Caro et al., 2005](#)). These seminal results have opened avenues for further analysis of helical-shaped AVG designs assuring optimized hemodynamic performances at the graft-vein anastomosis. Among them, [Zheng et al. \(2009\)](#) explored the impact of helix amplitude in helical graft performances, whereas [Van Canneyt et al. \(2013\)](#) reported the existence of a non-trivial relationship between helix turns number and disturbed shear at the graft-venous anastomosis in closed-loop AVG configurations. An innovative helical-shaped AVG design combining a small amplitude out-of-plane helical graft with an internal spiral inducer was also proposed ([Kabinejadian et al., 2016](#)), and a beneficial impact of the induced helical flow at the distal anastomosis hemodynamics was documented.

However, the beneficial hemodynamic effect of helical-shaped grafts is counteracted by a possible *in vivo* deformation of the helical geometry as a consequence of (1) graft overstretching during implantation, and/or (2) elongation under arterial pressure. These issues could decrease the AVG efficacy to promote IH- protective helical blood flow at the graft-venous anastomosis ([Huijbregts et al., 2007](#)).

Aiming at both preserving and ameliorating the beneficial impact of helical flow in reducing the hemodynamic-related IH risk at the distal anastomosis in AVGs, here we adopted computational fluid dynamics (CFD) to characterize the hemodynamic performance of innovative AVG designs, based on the use of an internal flow divider. The design strategy of the proposed AVGs was driven by the need to deliver helical flow features at the graft-vein anastomosis, preserving from the IH risk of failure while ensuring preservation of the graft geometry during and after implantation. The hemodynamic performances of six designed AVGs were compared with commercially available straight conventional, and a helical-shaped graft. Differences among the investigated designs in terms of hemodynamics developing at the graft-vein anastomosis were evaluated and a solution is proposed with the aim to reduce the risk of implant failure.

## Materials and Methods

### *AVG Design*

Eight different idealized 3D graft models connecting an artery and a vein in a closed-loop configuration were created in Solidworks. All models consisted of a 4 mm diameter artery, a 6 mm graft section and a 6 mm vein. Vessel length was equal to 90 mm, the closed-loop configuration length was equal to 300 mm, with anastomosis angles set to 45° (Figure 1).

Two of the eight models were constructed to reproduce the design of commercially available AVGs and were used as reference standard. These are a straight conventional graft (denoted S-AVG), and a helical-shaped graft (H-AVG) resembling the SwirlGraft™ (Veryan Medical Limited, UK). The latter design consists in 6 mm internal diameter (D), 3 mm (0.5 D) helix amplitude, and 70 mm (11.5 D) helix pitch ([Caro et al., 2005](#); [Van Canneyt et al., 2013](#)). The other six models presented a novel design. In detail, the section of the grafts was divided into three equal parts by positioning a 0.1 mm thickness flow divider (FD), as shown in Figure 1. For three models, named as linear flow divider (LFD) models, the FD was not rotated along the centerline of the graft, while in the other three models, named as helical flow divider (HFD) models, the FD is rotated while translated along the graft section, describing three helically-shaped segments around the graft centerline. Three AVG designs were considered for both LFD and HFD solutions by differently positioning the FD, as shown in Figure 1. The geometrical features of all models are summarized in Table S1 of the Supplementary Materials.

### *Computational Fluid Dynamics*

The finite volume-based CFD code Fluent (ANSYS Inc., USA) was used to solve the governing equations of fluids motion in their unsteady-state discrete form. For this aim, the AVG fluid

domain was discretized using ICEM (ANSYS Inc., USA) with tetrahedral elements in the lumen region, and with 10 (5 for models with FD) layers of high-quality prismatic elements in the near-wall region. An analysis of the sensitivity of the numerical solution to the cardinality of the mesh is presented in the Supplementary Materials.

Blood was considered as an incompressible, Newtonian fluid with density equal to  $1,060 \text{ kg/m}^3$  and dynamic viscosity equal to  $0.0035 \text{ Pa}\cdot\text{s}$  (Loth et al., 2008).

The scheme already proposed elsewhere (Van Canneyt et al., 2013) consistently with clinical recommendations (NKFK/DOQI, 2006; Tordoir et al., 2007) was applied to define conditions at boundaries. A measured post-operative flow rate waveform (Huberts et al., 2012) was scaled to obtain an average inflow rate value of  $600 \text{ mL/min}$  and prescribed in terms of flat velocity profile at the inflow section (proximal artery - PA). At outflow boundaries, flow ratios were prescribed: 90% of the inflow at the proximal vein (PV) outlet section, 5% at the distal vein (DV), and 5% at the distal artery (DA). The imposed flow waveforms are presented in Figure 2. Details on the applied numerical schemes are reported in the Supplementary Materials.

### *Hemodynamic Descriptors*

Near-wall hemodynamics was analyzed in terms of three well-established WSS-based descriptors of 'disturbed flow' (Table 1): time-averaged wall shear stress (TAWSS), oscillatory shear index (OSI) (Ku et al., 1985), and relative residence time (RRT) (Himburg et al., 2004). The analysis was focused at the region of interest (ROI) at the venous anastomosis (Figure 2). As in previous studies (Gallo et al., 2012, 2016), data from all cases were combined to define objective thresholds for 'disturbed flow'. From pooled data, the upper (lower) 20<sup>th</sup> percentile was identified for OSI and RRT (TAWSS). For each model, the percentage of ROI surface area (SA) exposed to OSI and RRT values higher (lower for TAWSS) than the defined thresholds was quantified. These SAs were labeled as OSI80,



RRT80, and TAWSS20. Moreover, the mean value of each WSS-based descriptor at the ROI was computed.

Intravascular hemodynamics was investigated in terms of amount and topology of helical flow, recognized (1) to suppress WSS disturbances (De Nisco et al., 2019; Gallo et al., 2012, 2015, 2018; Morbiducci et al., 2007, 2013), and (2) to reduce the hemodynamic risk of failure in AVGs (Caro et al. 2005, 2007; Van Canneyt et al., 2013). Table 1 reports the computed helicity-based descriptors. In detail, three descriptors evaluating strength, size and relative rotational direction of helical blood structures (Gallo et al., 2012) were calculated inside the graft segment: cycle-average helicity ( $h_1$ ) and helicity intensity ( $h_2$ ), quantifying respectively the net amount and the intensity of helical flow; unsigned ( $h_4$ ) helical rotation balance, indicating the presence of a dominant direction of rotation of helical blood structures. Furthermore, the local normalized helicity (LNH) (Morbiducci et al., 2007), representing the normalized internal product between local velocity and vorticity vectors, was used to visualize helical blood flow structures inside the investigated models. As LNH magnitude measures the alignment/misalignment of local velocity and vorticity vectors, while its sign indicates the direction of rotation of helical structures, LNH is useful to visualize left- and right-handed blood structures in the investigated domain.

Additionally, aware of the well-known increased risk of blood clotting in the graft (Jaffer et al., 2015), here regions of blood recirculation were quantitatively analyzed. To do that, the volume of recirculating flow in the AVG was computed as proposed elsewhere (Clark et al., 2015; Gallo et al., 2018; Martorell et al., 2014). In detail, the CFD-computed velocity vector field into the graft segment of each model was locally projected along the centerline (Morbiducci et al., 2015), and then the volume of all finite-volumes containing a mean negative axial velocity component was integrated. The obtained fluid volume was then normalized by the respective graft volume, and denoted VolRec (Gallo et al., 2018; Tasso et al., 2018).

## Results

The values of the WSS-based indicators, averaged over the ROI at the graft-venous side of each AVG design, are presented in Figure 3. The hemodynamics in model HFD-3 is characterized, in the venous anastomosis region: (1) the highest TAWSS, with values within the physiological range; (2) the lowest RRT and OSI (the latter comparable with the S-AVG model). Interestingly, in general OSI values at ROI are very low in all the investigated AVG models (Figure 3), suggesting that WSS directionality does not markedly characterize local hemodynamics in the distal vein region. A more direct comparison is provided in Figure 4. Considering the percentage differences in WSS-based descriptors values averaged over the ROI surface area, it emerges that the H-AVG presents better performances than S-AVG (+3.4% and -13.8% in ROI-averaged TAWSS and RRT values, respectively), therefore reducing the hemodynamic-related risk of IH formation. The comparison of the designed grafts with S-AVG and H-AVG (Figure 4) highlights that, overall, S-AVG and H-AVG perform better than LFD models, in terms of IH hemodynamic risk. Moreover, in the novel AVG designs, ROI-average OSI values are higher than in the S-AVG device (up to 90.7%, case LFD-2), except for case HFD-3 (-1%). Case HFD-3 also presents lower ROI-averaged OSI values than H-AVG model (-38.1%). Additionally, model HFD-3 presents ROI-average TAWSS the 38.8% and 34.2% higher, and RRT the 38.9% and 29.1% lower, than S-AVG and H-AVG models, respectively. This suggests a lower hemodynamic risk of IH at the venous anastomosis for case HFD-3. Helical models HFD-1 and HFD-2 perform overall less effectively than S-AVG and H-AVG.

An evaluation of the impact of AVG design on IH-related risk of failure is also provided in terms of the fraction of the ROI surface area exposed to disturbed shear (Figure 5). By visual inspection, in the ROI: (1) LFD grafts present the largest exposure to low WSS (TAWSS<sub>20</sub>) and high RRT (RRT<sub>80</sub>); (2) HFD-1 and HFD-2 grafts present lower exposure to low WSS and high RRT than S-AVG, but larger than H-AVG; (3) model HFD-3 presents the lowest SAs exposed to disturbed shear,

performing better than the conventional straight graft S-AVG and the helical-shaped graft H-AVG. These observations are confirmed by the quantitative data summarized in Table S3 of the Supplemental data.

Insights into the impact of different AVG designs in promoting or suppressing the hemodynamic risk of IH at the venous anastomosis can be given by in-graft and intravascular flow patterns. Helical blood flow patterns developing into the AVG models are visualized in Figure 6 using isosurfaces of cycle-average LNH (at  $\pm 0.4$ ), where blue and red colors indicate respectively left-handed and right-handed helical flow rotation (Gallo et al., 2012; Morbiducci et al., 2013). Notably, distinguishable helical flow structures characterize the flow into the grafts and in the region of the graft-vein anastomosis, but their peculiar features are dependent on graft and FD geometry, and on FD position (Figure 6). In particular, considering the whole graft, it can be observed that: (1) as expected, H-AVG is characterized by the highest helical flow intensity ( $h_2 = 50.844 \text{ m/s}^2$ ); (2) balanced and separated counter-rotating blood structures appear in the S-AVG and LFD models ( $h_4 = 0.044$  for S-AVG and ranging from 0.001 to 0.015 for LFD grafts); (3) counter-rotating helical blood structures characterize the intravascular flow in H-AVG and HFD grafts, but they are more unbalanced than the other models ( $h_4$  values ranging from 0.155 for HFD-2 to 0.300 in H-AVG). The values of the helicity-based descriptors are reported in the Supplemental data (Table S4).

Most of the investigated AVG geometries promote the development of two or more rotating blood structures in the graft-vein anastomosis region. An exception to this is represented by models H-AVG and HFD-3, in which helical blood flow with a predominant rotating direction is conveyed at the venous side (Figure 6). This unbalanced helical flow pattern leads to a more effective washout at the wall in the distal vein, explaining the reduced amount of low and oscillatory WSS found there in H-AVG and HFD-3 models, as suggested by RRT80 maps in Figure 5.

A visual inspection of the lumen cross-sectional velocity patterns at peak systole (Figure 7) confirms this statement, highlighting the presence of low velocity regions downstream of the venous anastomosis. The extension of those low velocity regions, typically associated with flow separation and recirculation, is markedly dependent upon helical flow patterns: (1) in general, the helical-shaped graft H-AVG and the HFD grafts present smaller low velocity regions than the straight conventional and LFD grafts; (2) graft HFD-3 presents the smaller near-wall low velocity region, and a velocity pattern characterized by one large secondary flow structure and higher axial velocities, close to the ROI.

The hemodynamic performance of the grafts is further assessed with the analysis of the risk of thrombus formation in terms of amount of blood recirculation. The quantification of the recirculating flow, displayed in Figure 8 (left panel), highlights that: (1) the percentage volume of recirculation in the graft is low in all the investigated AVG models (VolRec <1% in all models); (2) the insertion of a FD does not result in a marked increased risk of thrombus formation, as can be noted comparing VolRec values in LFD or HFD grafts vs. S-AVG and H-AVG, respectively (Figure 8, left panel).

To complete the hemodynamic characterization of the different AVG designs, the cycle-average pressure drops over the graft segment are presented in Figure 8 (right panel). As expected, the insertion of the FD and the helically-shaped geometry affects the energetics of blood flowing in the graft. The conventional straight S-AVG is characterized by the lowest pressure drop. As expected, the longer is the FD, the higher the pressure drop, and helically-shaped FDs add a further contribution. Model HFD-3, the graft associated with the lowest IH hemodynamic risk at the venous anastomosis, is characterized by a pressure drop over the graft segment 3.8 mmHg and 2.0 mmHg higher than the conventional S-AVG and H-AVG, respectively.

## Discussion

The use of AVGs as permanent vascular access for hemodialysis patients is still associated with a significant failure rate, mainly due to IH developing at the distal venous anastomosis ([Ene-Iordache and Remuzzi, 2017](#); [Shiu et al., 2019](#)), promoted by 'disturbed' hemodynamics ([Allon, 2007](#); [Beathard, 2002](#); [Li et al., 2008](#); [Loth et al., 2003, 2008](#); [Maya et al., 2004](#); [Roy-Chaudhury et al., 2001, 2006](#)). Aiming at avoiding the establishment of disturbed flow patterns, researchers proposed novel AVGs equipped with an out-of-plane helical segment ([Caro et al., 2005, 2007](#); [Kabinejadian et al., 2016](#)). However, the efficacy of these devices in promoting helical flow developing at the distal anastomosis could be markedly affected by *in vivo* deformation during implantation ([Huijbregts et al., 2007](#)).

Moving from the insights from those previous studies, here we explored alternative designs of AVG (Figure 1) with the aim to reduce the hemodynamic-related, clinically relevant IH risk at the distal anastomosis leveraging the recognized beneficial role played by helical flow in minimizing blood flow disturbances. The alternative AVG designs are based on the consideration of a FD inside the graft, which could be straight or helical-shaped, with different length and location.

Using computational fluid dynamics, the hemodynamic performance of the newly designed AVGs was evaluated against commercially available AVG models. A sketch summarizing the findings of the study is presented in Figure 9, where AVGs performance is evaluated with respect to the commercially available, conventional straight graft model (S-AVG). It clearly emerges that the insertion of a helical-shaped FD shorter than the graft located at the venous side (model HFD-3) promotes beneficial helical flow patterns at the venous anastomosis (Figure 6) that, reducing disturbed shear (Figure 3, 4, 5), lower the related risk of IH formation ([Kabinejadian et al., 2016](#); [Van Canneyt et al., 2013](#); [Ene-Iordache and Remuzzi, 2017](#)). For the sake of completeness, a more extensive analysis taking in account other possible unfavorable hemodynamic effects related to

the adoption of such an AVG design was conducted (Figure 8). Despite the introduced new geometric AVG features could have a detrimental impact on graft potential thrombosis risk and graft resistance to flow (consistently with [Liu et al., 2016](#); [Van Canneyt et al., 2013](#)), a quantitative comparison of model HFD-3 with the two commercially-available grafts S-AVG and H-AVG revealed that this detrimental impact, when present, does not have clinical relevance ( $\text{VolRec} < 0.6\%$ , against a  $\text{VolRec}$  of 0.4% and 0.8% for S-AVG and H-AVG, respectively; pressure drop 2.0 mmHg higher than S-AVG, and 3.8 mmHg lower than H-AVG). All these evidences suggested model HFD-3 as a potential strategy to reduce IH-related complications of commercial AVGs.

An additional advantage of adopting a helical shape for the newly-proposed HFD grafts is in the possibility of exploiting the helical flow property of stabilizing the flow field at the venous anastomosis, thus avoiding transition to turbulence ([Moffat and Tsinober, 1992](#); [Morbidity et al., 2011](#)). The consequence for this design-driving choice is in the minimization of the risk of the onset of transition to turbulence at the AVG venous side, as observed in previous studies considering straight conduits ([Loth et al., 2003](#); [Lee et al., 2007](#); [Broderick et al., 2015](#)). Here, we assumed flow laminarity. This assumption is based upon (1) the favourable, clinically suggested flow division between proximal and distal segments ([Lee et al., 2007](#); [Broderick et al., 2015](#)), and (2) the stabilizing effect of the induced helical flow on the hemodynamics at the venous anastomosis ([Moffat and Tsinober, 1992](#); [Morbidity et al., 2011](#)). Based on that, the onset of transitional flow in the proposed helical-shaped AVG designs is unlikely.

Several limitations could weaken the findings of this study. In particular, here the graft models, in a closed-loop configuration, and the host vessels were simplified as idealized geometries and their wall were assumed to be rigid. However, the idealized model-based approach enables to clearly identify if and to which extent AVG geometry promotes IH-prone hemodynamic phenotypes, by varying one specific graft geometrical feature at time. As for the rigid-wall assumption, we

consider this approximation to be reasonable because of the low pressure variation in the AV graft, and the moderate compliance of veins and synthetic grafts ([Loth et al., 2003](#)). Moreover, the idealization introduced considering graft and vessels as rigid conduits is justified by previous findings, in relation to WSS ([Ene-Iordache and Remuzzi, 2017](#); [Ngoepe et al., 2011](#)).

The aim of this study was to evaluate the general applicability of the newly proposed AVG design, and its potential beneficial role in reducing the hemodynamic-related risk of IH development at the venous anastomosis. Hence, the impact of outflow ratio and anastomosis angle variation were not investigated here. However, an anastomosis angle of 45° was here investigated in order to evaluate the AVGs design in a suboptimal hemodynamic operating condition, thus proving more effectively the beneficial impact of an optimized helical design in mitigating AVG hemodynamic-related risks, by minimizing flow instabilities.

Moreover, no graft parametric study ([Sun et al., 2010](#); [Zhan et al., 2010](#)) was conducted to optimize the geometric design of the helical-shaped FD. However, the adopted design solution was dictated here by previous findings ([Van Canneyt et al., 2013](#)), and by the fact that, in terms of energetics, increasing the number of helix turns leads to (1) increased pressure losses, and (2) increased risk of thrombus formation in the graft. Finally, here we considered a FD thickness of 0.1 mm to limit AVG cross-sectional area reduction and, ultimately, the risk of thrombus formation. Such design choice is supported by recently proposed ultralow profile, thromboresistant superelastic materials used for endograft in small vessels ([Shayan et al., 2017](#)). To expand the analysis to production techniques based on extrusion or 3D printing, we additionally considered a FD thickness equal to 0.5 mm (Supplemental data, Figure S1) in HFD-3 model. A larger FD thickness (1) does not increase the associated hemodynamic-based IH risk, (2) expectedly leads to a very modest increase in the risk of thrombus formation (quantified by VolRec, that is however lower than in the commercial device H-AVG case). As woven fabrics for vascular applications with

thickness down to 0.25 mm are already commercially available (see, e.g., the De Bakey woven ([Rajendran and Anand, 2012](#))), we can conclude that the proposed AVG graft design with thickness in the range 0.1 - 0.5 mm could be currently fabricated.

## Conclusion

Here we identify aAVG design based on the consideration of an internal-to-graft helical-shaped FD located at the venous side. By inducing beneficial helical flow patterns, the proposed AVG design reduces disturbed shear and, as a consequence, the associated hemodynamic-based IH risk at the distal vein, without markedly increasing pressure drop and the risk of thrombus formation. By construction, the alternative AVG design is less sensitive than commercially available helical-shaped AVGs to during and post-implantation deformation. As the purpose of this study was to numerically explore the potential hemodynamic risk associated with alternative AVG designs, the presented findings need to be confirmed by animal tests.



## REFERENCES

- Allon, M., 2007. Current management of vascular access. *Clinical Journal of American Society of Nephrology* 2, 786-800.
- Bassiouny, H.S., White, S., Glagov, S., Choi, E., Giddens, D.P., Zarins, C.K., 1992. Anastomotic intimal hyperplasia: mechanical injury or flow induced. *Journal of Vascular Surgery* 15(4), 708-716.
- Beathard, G.A., 2002. Angioplasty for arteriovenous grafts and fistulae. *Seminars in Nephrology* 22, 202-210.
- Bechara, C.F., 2014. Comparing short and midterm Infrainguinal bypass patency rates between two ePTFE prosthetic grafts: spiral laminar flow and propaten. *Vascular Disease Management* 11, E54-E58.
- Bogren, H.G., Buonocore, M.H., 1994. Blood flow measurements in the aorta and major arteries with MR velocity mapping. *Journal of Magnetic Resonance Imaging* 4(2), 119-30.
- Broderick, S.P., Houston, J.G., Walsh, M.T., 2015. The influence of the instabilities in modelling arteriovenous junction haemodynamics. *Journal of biomechanics* 48(13), 3591-3598.
- Caro, C., Cheshire, N., Watkins, N., 2005. Preliminary comparative study of small amplitude helical and conventional ePTFE arteriovenous shunts in pigs. *Journal of the Royal Society Interface* 2, 261-266.
- Caro, C., Doorly, D., Tarnawski, M., Scott, K., Long, Q., Dumoulin, C., 1996. Non- planar curvature and branching of arteries and non-planar-type flow. *Proceedings of the Royal Society of London Series A: Mathematical Physical and Engineering Sciences* 452, 185-197.
- Caro, C., Fitz-Gerald, J., Schroter, R., 1971. Atheroma and arterial wall shear. Observation, correlation and proposal of a shear dependent mass transfer mechanism for atherogenesis. *Proceedings of the Royal Society: Biological Sciences* 177(46), 109-159.
- Caro, C., Watkins, N., Sherwin, S., 2007. Helical graft. Patent US 2007/0021707 A1 (2007).
- Clark, T.W., Isu, G., Gallo, D., Verdonck, P., Morbiducci, U., 2015. Comparison of symmetric hemodialysis catheters using computational fluid dynamics. *Journal of Vascular and Interventional Radiology* 26(2), 252-259.
- Coppola, G., Caro, C., 2009. Arterial geometry, flow pattern, wall shear and mass transport: potential physiological significance. *Journal of the Royal Society Interface* 6, 519-528.
- Cunnane, C.V., Cunnane, E.M., Walsh, M.T., 2017. A review of the hemodynamic factors believed to contribute to vascular access dysfunction. *Cardiovascular Engineering and Technology* 8(3), 280-294.
- De Nisco, G., Kok, A.M., Chiastra, C., Gallo, D., Hoogendoorn, A., Migliavacca, F., Wentzel, J.J., Morbiducci, U., 2019. The atheroprotective nature of helical flow in coronary arteries. *Annals of Biomedical Engineering* 47(2), 425-438.

Dixon, B.S., Beck, G.J., Vazquez, M.A., Greenberg, A., Delmez, J.A., Allon, M., Dember, L.M., Himmelfarb, J., Gassman, J.J., Greene, T., Radeva, M.K., Davidson, I.J., Ikizler, T.A., Braden, G.L., Fenves, A.Z., Kaufman, J.S., Cotton, J.R.Jr, Martin, K.J., McNeil, J.W., Rahman, A., Lawson, J.H., Whiting, J.F., Hu, B., Meyers, C.M., Kusek, J.W., Feldman, H.I., 2009. Effect of dipyridamole plus aspirin on hemodialysis graft patency. *The New England Journal of Medicine* 360, 2191-2201.

Ene-lordache, B., Remuzzi, A., 2017. Blood Flow in Idealized Vascular Access for Hemodialysis: A Review of Computational Studies. *Cardiovascular Engineering and Technology* 8(3), 295-312.

Gallo, D., Bijari, P.B., Morbiducci, U., Qiao, Y., Xie, Y., Etesami, M., Haabets, D., Lakatta, E.G., Wasserman, B.A., Steinman, D.A., 2018. Segment-specific associations between local haemodynamic and imaging markers of early atherosclerosis at the carotid artery: an in vivo human study. *Journal of the Royal Society Interface* 15 (147), 20180352.

Gallo, D., Steinman, D.A., Bijari, P.B., Morbiducci, U., 2012. Helical flow in carotid bifurcation as surrogate marker of exposure to disturbed shear. *Journal of Biomechanics* 45, 2398–2404.

Gallo, D., Steinman, D.A., Morbiducci, U., 2015. An insight into the mechanistic role of the common carotid artery on the hemodynamics at the carotid bifurcation. *Annals of Biomedical Engineering*, 43(1), 68-81.

Gallo, D., Steinman, D.A., Morbiducci, U., 2016. Insights into the co-localization of magnitude-based versus direction-based indicators of disturbed shear at the carotid bifurcation. *Journal of Biomechanics* 49(12), 2413-9.

Himburg, H.A., Grzybowski, D.M., Hazel, A., LaMack, J.A., Li, X.M., Friedman, M.H., 2004. Spatial comparison between wall shear stress measures and porcine arterial endothelial permeability. *American Journal of Physiology-Heart and Circulatory Physiology* 286, H1916-H1922.

Hodges, T., Fillinger, M., Zwolak, R., Walsh, D., Bech, F., Cronenwett, J., 1997. Longitudinal comparison of dialysis access methods: risk factors for failure. *Journal of Vascular Surgery* 26, 1009-1019.

Huberts, W., Bode, A., Kroon, W., Planken, R., Tordoir, J., van de Vosse, F., Bosboom, E., 2012. A pulse wave propagation model to support decision-making in vascular access planning in the clinic. *Medical Engineering and Physics* 34, 233-248.

Huijbregts, H., Blankestijn, P., Caro, C., Cheshire, N., Hoedt, M., Tutein Nolthenius, R.P., Moll, F., 2007. A helical PTFE arteriovenous access graft to swirl flow across the distal anastomosis: results of a preliminary clinical study. *European Journal of Vascular and Endovascular Surgery* 33, 472-475.

Jaffer, I.H., Fredenburgh, J.C., Hirsh, J., 2015. Medical device-induced thrombosis: what causes it and how can we prevent it? *Journal of Thrombosis and Haemostasis* 13(S1), S72-S81.

- Kabinejadian, F., McElroy, M., Ruiz-Zoler, A., Leo, H.L., Slevin, M.A., Badimon, L., Keshmiri, A., 2016. Numerical assessment of novel helical/spiral grafts with improved hemodynamics for distal graft anastomoses. *PLoS ONE* 11(11), e0165892.
- Kelly, B.S., Heffelfinger, S.C., Whiting, J.F., Miller, M.A., Reaves, A., Armstrong, J., Narayana, A., Roy-Chaudhury, P., 2002. Aggressive venous neointimal hyperplasia in a pig model of arteriovenous graft stenosis. *Kidney International* 62, 2272-2280.
- Ku, D.N., Giddens, D.P., Phillips, D.J., Strandness, D.E. Jr, 1985. Hemodynamics of the normal human carotid bifurcation: in vitro and in vivo studies. *Ultrasound in Medicine & Biology* 11(1), 13-26.
- Lee, S.W., Antiga, L., Steinman, D., 2009. Correlations among indicators of disturbed flow at the normal carotid bifurcation. *Journal of Biomechanical Engineering* 131, 061013.
- Lee, S.W., Smith, D.S., Loth, F., Fisher, P., Bassiouny, H.S., 2007. Importance of flow division on transition to turbulence within an arteriovenous graft. *Journal of biomechanics* 40(5), 981-992.
- Li, L., Terry, C.M., Shiu, Y.T.E., Cheung, A.K., 2008. Neointimal hyperplasia associated with synthetic hemodialysis grafts. *International Society of Nephrology* 74, 1247-1261.
- Liu, X., Sun, A., Fan, Y., Deng, X., 2015. Physiological significance of helical flow in the arterial system and its potential clinical applications. *Annals of Biomedical Engineering* 43(1), 3-15.
- Liu, X., Wang, L., Wang, Z., Li, Z., Kang, H., Fan, Y., Sun, A., Deng, X., 2016. Bioinspired helical graft with taper to enhance helical flow. *Journal of Biomechanics* 49, 3643-3650.
- Loth, F., Fischer, P., Bassiouny, S., 2008. Blood flow in end-to-side anastomoses. *Annual Review of Fluid Mechanics* 40, 367-393.
- Loth, F., Fischer, P.F., Arslan, N., Bertram, C.D., Lee, S.E., Royston, T.J., Shaalan, W.E., Bassiouny, H.S., 2003. Transitional flow at the venous anastomosis of an arteriovenous graft: potential activation of the ERK1/2 mechanotransduction pathway. *Journal of Biomechanical Engineering* 125(1): 49-61.
- Martorell, J., Santoma, P., Kolandaivelu, K., Kolachalama, V.B., Melgar-Lesmes, P., Molins, J.J., Garcia, L., Edelman, E.R., Balcels, M., 2014. Extent of flow recirculation governs expression of atherosclerotic and thrombotic biomarkers in arterial bifurcations. *Cardiovascular Research* 103, 37-46.
- Maya, I.D., Oser, R., Saddekni, S., Barker, J., Allon, M., 2004. Vascular access stenosis: comparison of arteriovenous grafts and fistulas. *American Journal of Kidney Disease* 44, 859-865.
- Moffatt, H.K., Tsinober, A., 1992. Helicity in laminar and turbulent flow. *Annual review of fluid mechanics* 24(1), 281-312.
- Morbiducci, U., Gallo, D., Cristofanelli, S., Ponzini, R., Deriu, M.A., Rizzo, G., Steinman, D.A., 2015. A rational approach to defining principal axes of multidirectional wall shear stress in realistic

vascular geometries, with application to the study of the influence of helical flow on wall shear stress directionality in aorta. *Journal of Biomechanics* 48(6), 899-906

Morbiducci, U., Ponzini, R., Gallo, D., Bignardi, C., Rizzo, G., 2013. Inflow boundary conditions for image-based computational hemodynamics: impact of idealized versus measured velocity profiles in the human aorta. *Journal of Biomechanics* 46, 102-109.

Morbiducci, U., Ponzini, R., Grigioni, M., Redaelli, A., 2007. Helical flow as fluid dynamic signature for atherogenesis in aortocoronary bypass. A numeric study. *Journal of Biomechanics* 40, 519-534.

Morbiducci, U., Ponzini, R., Rizzo, G., Cadioli, M., Esposito, A., Montevecchi, F.M., Redaelli, A., 2011. Mechanistic insight into the physiological relevance of helical blood flow in the human aorta: an in vivo study. *Biomechanics and modeling in mechanobiology* 10(3), 339-355.

Ngoepe, M.N., Reddy, B.D., Kahn, D., Meyer, C., Zilla, P., Franz, T., 2011. A Numerical Tool for the Coupled Mechanical Assessment of Anastomoses of PTFE Arteriovenous Access Grafts. *Cardiovascular Engineering and Technology* 2(3), 160-172.

NKF-K/DOQI, 2006. Clinical practice guidelines for vascular access: update 2006. *American Journal of Kidney Diseases* 48 (Suppl. 1), S248-S273.

Ojha, M., 1993. Spatial and temporal variations of wall shear stress within an end-to-side arterial anastomosis model. *Journal of Biomechanics* 26(12), 1377-1388.

Pisoni, R.L., Zepel, L., Port, F.K., Robinson, B.M., 2015. Trends in US vascular access use, patient preferences, and related practices: an update from the US DOPPS practice monitor with international comparisons. *American Journal of Kidney Disease* 65, 905-915.

Rajendran, S., Anand, S.C., 2012. Woven textiles for medical applications. In: Gandhi K.L. (Eds.), *Woven Textiles. Principles, Technologies and Applications*. Woodhead Publishing, Cambridge, pp. 414-441.

Rittgers, S., Karayannacos, P., Guy, J., Nerem, R., Shaw, G., Hostetler, J., Vasko, J., 1978. Velocity distribution and intimal proliferation in autologous vein grafts in dogs. *Circulation Research* 42, 792-801.

Roy-Chaudhury, P., Kelly, B.S., Miller, M.A., Reaves, A., Armstrong, J., Nanayakkara, N., Heffelfinger, S.C., 2001. Venous neointimal hyperplasia in polytetrafluoroethylene dialysis grafts. *Kidney International* 59, 2325-2334.

Roy-Chaudhury, P., Spergel, L., Besarab, A., Asif, A., Ravani, P., 2007. Biology of arteriovenous fistula failure. *Journal of Nephrology* 20, 150-163.

Roy-Chaudhury, P., Sukhatme, V., Cheung, A., 2006. Hemodialysis vascular access dysfunction: a cellular and molecular viewpoint. *Journal of the American Society of Nephrology* 17, 1112-1127.

Scott, E., Glickman, M., 2007. Conduits for hemodialysis access. *Seminars in Vascular Surgery* 20, 158-163.

- Sequeira, A., Naljayan, M., Vachharajani, T.J., 2017. Vascular access guidelines: Summary, rationale, and controversies. *Techniques in Vascular and Interventional Radiology* 20(1), 2-8.
- Shayan, M., Yang, S., Ryu, W., Chun, Y., 2017. A novel low-profile thin-film nitinol/silk endograft for treating small vascular diseases. *Journal of Biomedical Materials Research Part B Applied Biomaterials* 105(3):575-584.
- Sherwin, S.J., Shah, O., Doorly, D.J., Peirò, J., Papaharilaou, Y., Watkins, N., Caro, C.G., Dumoulin, C.L., 2000. The influence of out-of-plane geometry on the flow within a distal end-to side anastomosis. *Journal of Biomechanical Engineering* 122, 86-95.
- Shiu, Y.T., Rotmans, J.I., Geelhoed, W.J., Pike, D.B., Lee, T., 2019. Arteriovenous conduits for hemodialysis: how to better modulate the pathophysiological vascular response to optimize vascular access durability. *American Journal of Physiology-Renal Physiology*. (doi: 10.1152/ajprenal.00440)
- Stonebridge, P.A., Hoskins, P.R., Allan, P.L., Belch, J.F., 1996. Spiral laminar flow in vivo. *Clinical Science* 91(1), 17-21.
- Sun, A., Fan, Y., Deng, X., 2010. Numerical comparative study on the hemodynamic performance of a new helical graft with noncircular cross section and Swirlgraft. *Artificial organs* 34(1), 22-27.
- Tasso, P., Raptis, A., Matsagkas, M., Lodi Rizzini, M., Gallo, D., Xenos, M., Morbiducci, U., 2018. Abdominal aortic aneurysm endovascular repair: profiling post-implantation morphometry and hemodynamics with image-based computational fluid dynamics. *Journal of Biomechanical Engineering* 140(11), 111003.
- Tordoir, J., Canaud, B., Haage, P., Konner, K., Basci, A., Fouque, D., Kooman, J., Martin-Malo, A., Pedrini, L., Pizzarelli, F., Tattersall, J., Vennegoor, M., Wanner, C., ter Wee, P., Vanholder, R., 2007. EBPG on vascular access. *Nephrology, Dialysis, Transplantation* 22 (Suppl. 2), 88–117.
- Van Canneyt, K., Morbiducci, U., Eloot, S., De Santis, G., Segers, P., Verdonck, P., 2013. A computational exploration of helical arterio-venous graft designs. *Journal of Biomechanics* 46(2), 345-353.
- Wen, J., Zheng, T., Jiang, W., Deng, X., Fan, Y., 2011. A comparative study of helical-type and traditional-type artery bypass grafts: numerical simulation. *ASAIO Journal* 57,399-406.
- Zhan, F., Fan, Y., Deng, X., Xu, Z., 2010. The beneficial effect of swirling flow on platelet adhesion to the surface of a sudden tubular expansion tube: its potential application in end-to-end arterial anastomosis. *ASAIO Journal* 56(3), 172-179.
- Zheng, T., Fan, Y., Xiong, Y., Jiang, W., Deng, X., 2009. Hemodynamic performance study on small diameter helical grafts. *ASAIO Journal* 55, 192-199.

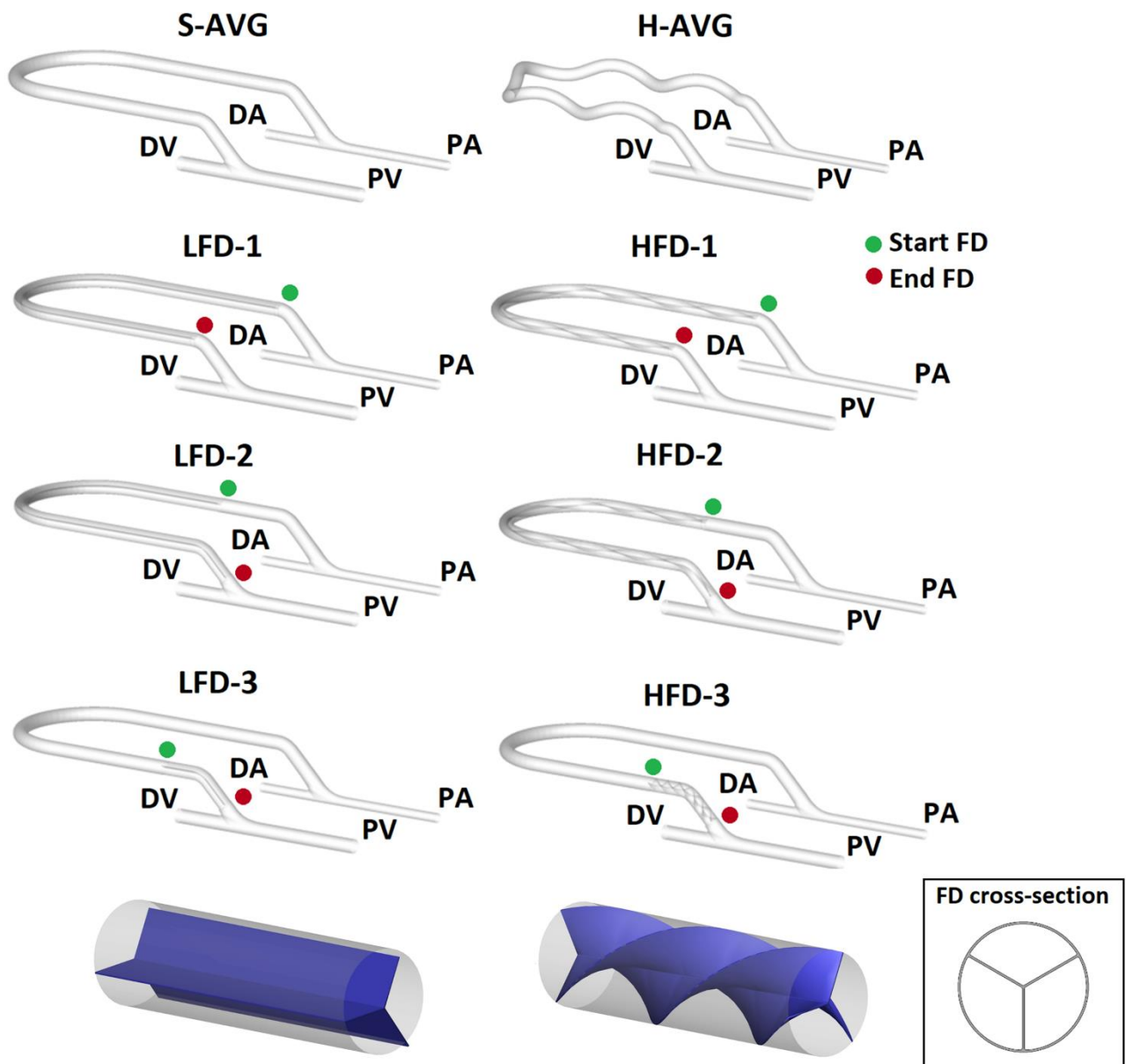
## Tables - Materials and Methods section

**Table 1.** Near-wall and intravascular hemodynamic descriptors

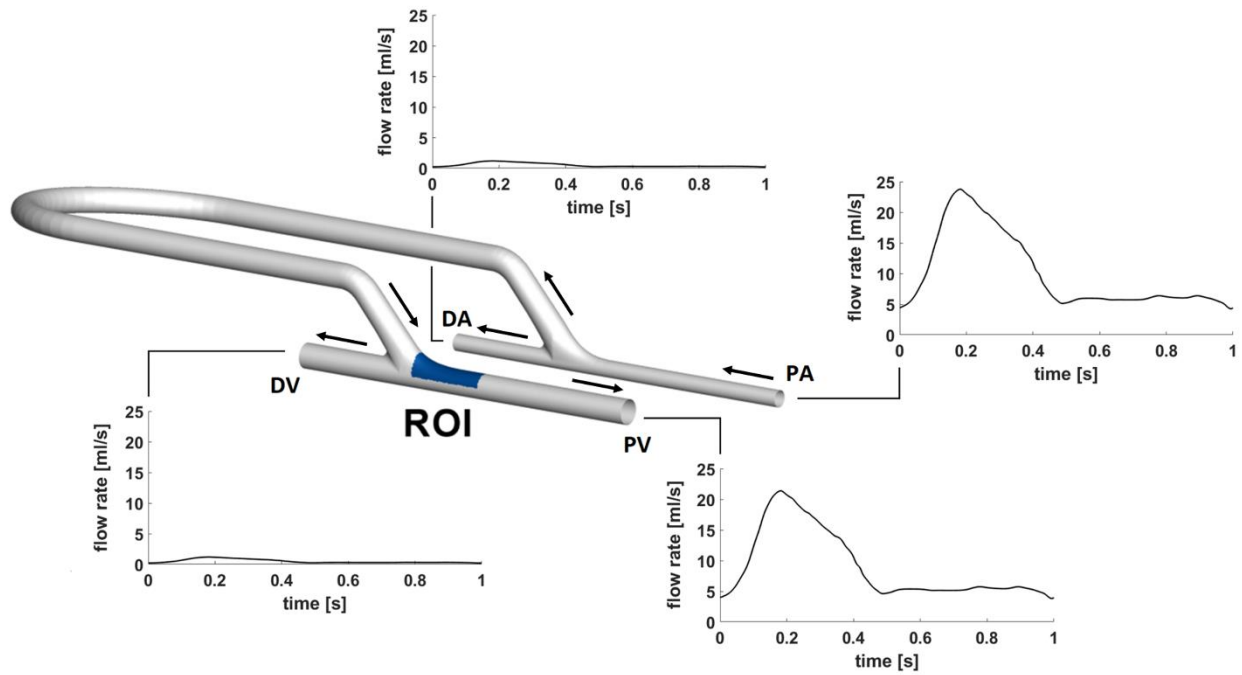
Time-Averaged WSS (TAWSS)	$\text{TAWSS} = \frac{1}{T} \int_0^T  \mathbf{WSS}  dt$
Oscillatory Shear Index (OSI)	$\text{OSI} = 0.5 \left[ 1 - \left( \frac{\left  \int_0^T \mathbf{WSS} dt \right }{\int_0^T  \mathbf{WSS}  dt} \right) \right]$
Relative Residence Time (RRT)	$\text{RRT} = \frac{1}{\text{TAWSS} \cdot (1 - 2 \cdot \text{OSI})} = \frac{1}{\frac{1}{T} \left  \int_0^T \mathbf{WSS} dt \right }$
Average Helicity ( $h_1$ )	$h_1 = \frac{1}{TV} \int_T \int_V \mathbf{v} \cdot \boldsymbol{\omega} dV dt$
Average Helicity Intensity ( $h_2$ )	$h_2 = \frac{1}{TV} \int_T \int_V  \mathbf{v} \cdot \boldsymbol{\omega}  dV dt$
Unsigned balance of counter-rotating helical flow structures ( $h_4$ )	$h_4 = \frac{ h_1 }{h_2} \quad 0 \leq h_4 \leq 1$
Local Normalized Helicity (LNH)	$\text{LNH} = \frac{\mathbf{v} \cdot \boldsymbol{\omega}}{ \mathbf{v}  \cdot  \boldsymbol{\omega} } = \cos \gamma$

**WSS** is the WSS vector;  $T$  is the period of the cardiac cycle;  $V$  is the model volume;  $\mathbf{v}$  is the velocity vector;  $\boldsymbol{\omega}$  is the vorticity vector.

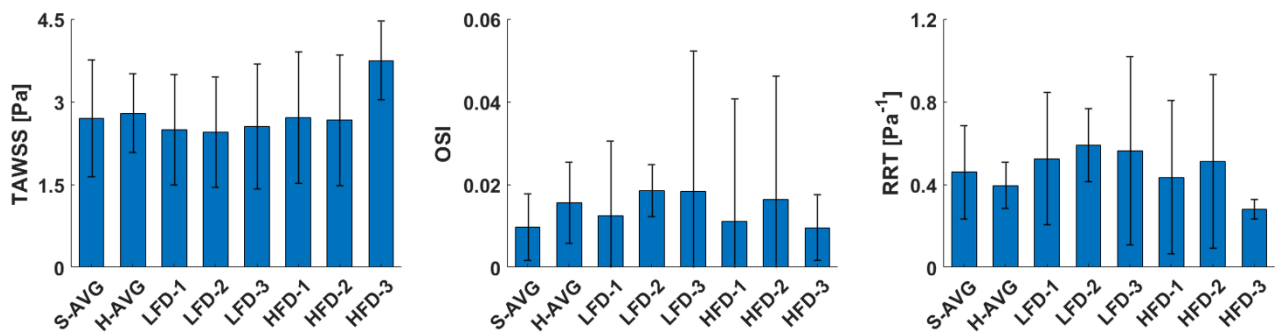
Figure captions



**Figure 1.** Investigated AVG models. Green and red markers indicate respectively the proximal and the distal end of the graft segment where the flow divider is present. Explanatory examples of linear and helical FD insertion are provided in the bottom panel. An axial cross-section of flow divider is also shown (bottom-right box). PA: proximal artery; DA: distal artery; PV: proximal vein; DV: distal vein.

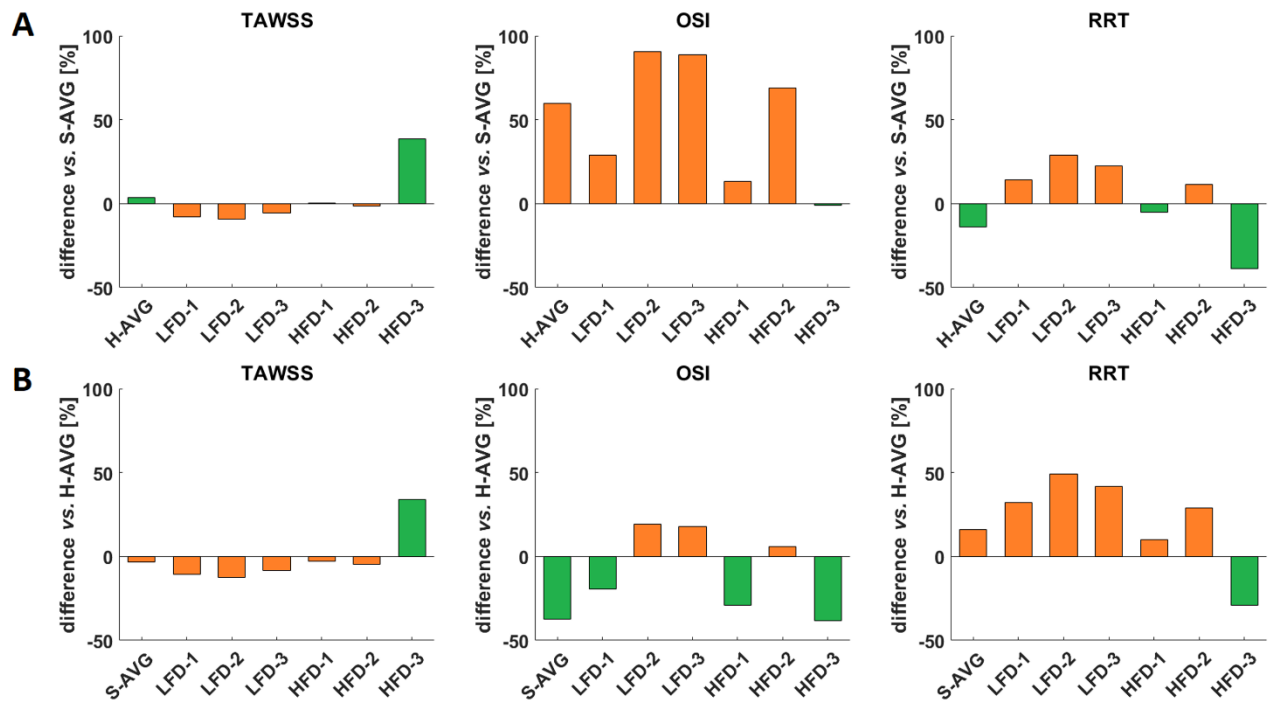


**Figure 2.** Volume flow rate waveforms prescribed as inflow and outflow conditions. The region of interest (ROI) at the venous anastomosis is coloured by blue. Blood flow direction is visualized by arrows. PA: proximal artery; DA: distal artery; PV: proximal vein; DV: distal vein.

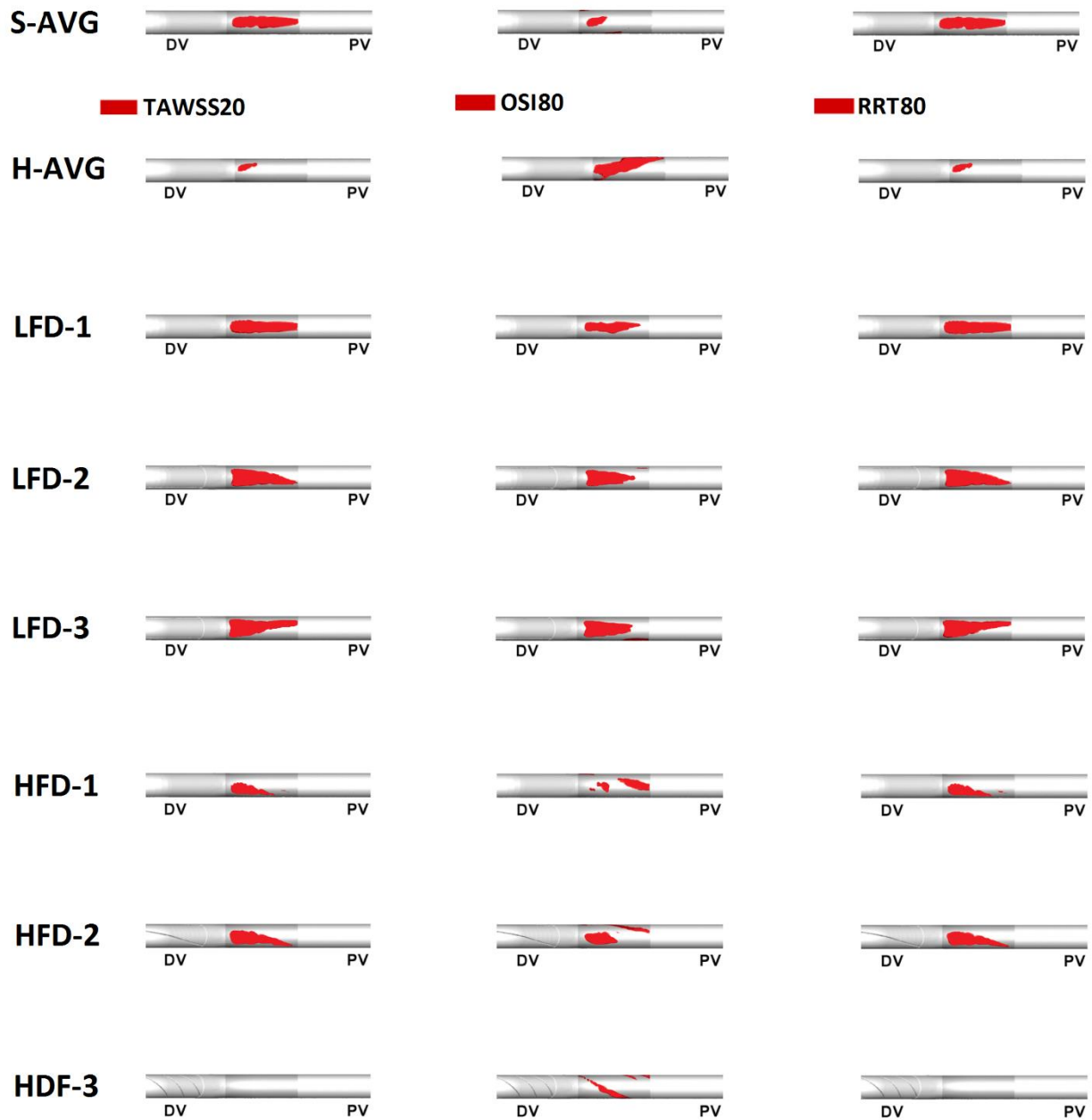


**Figure 3.** Mean values of WSS-based descriptors (TAWSS, OSI, and RRT) at the ROI. Vertical bars indicate  $\pm$  one standard deviation range.

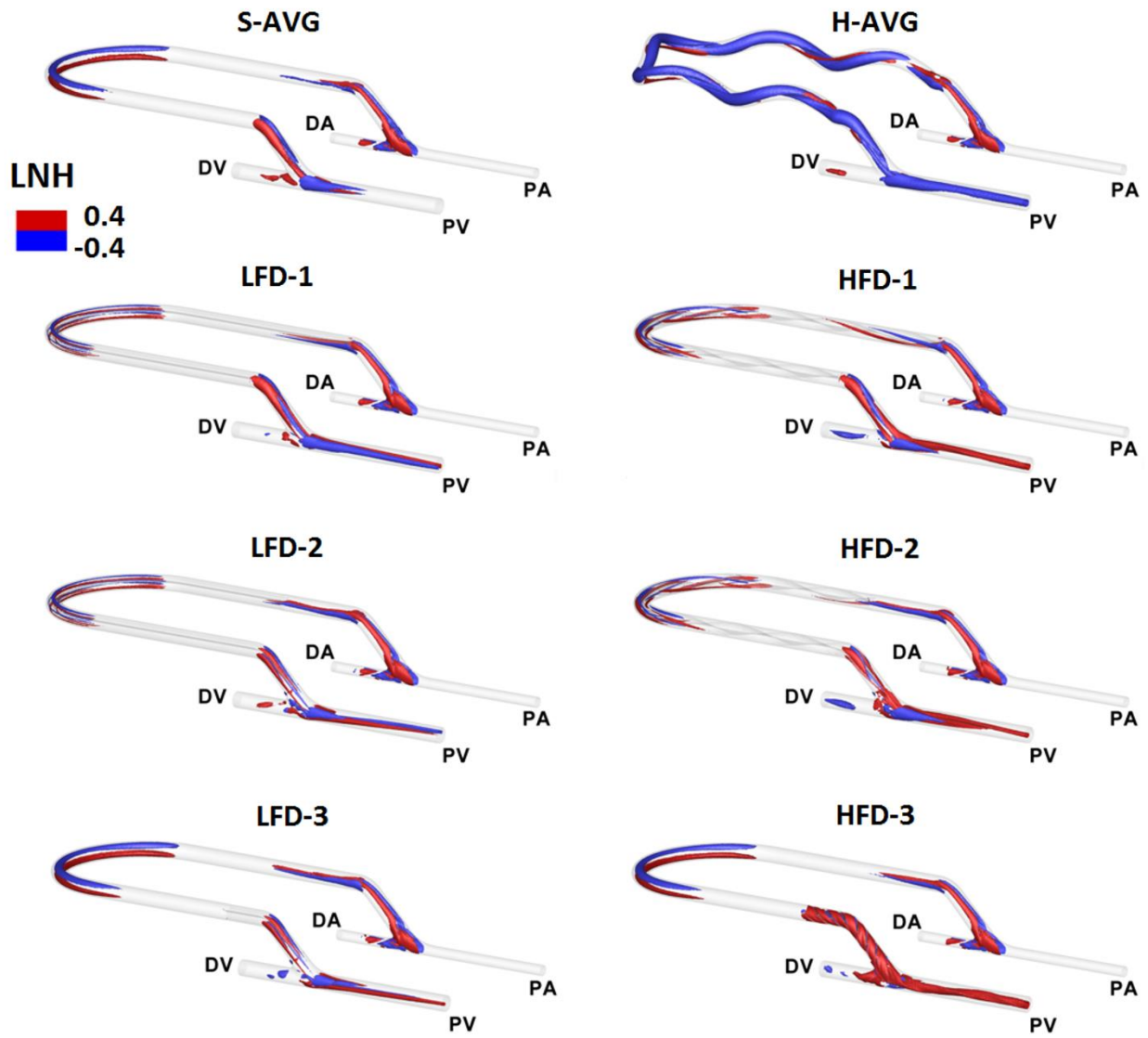




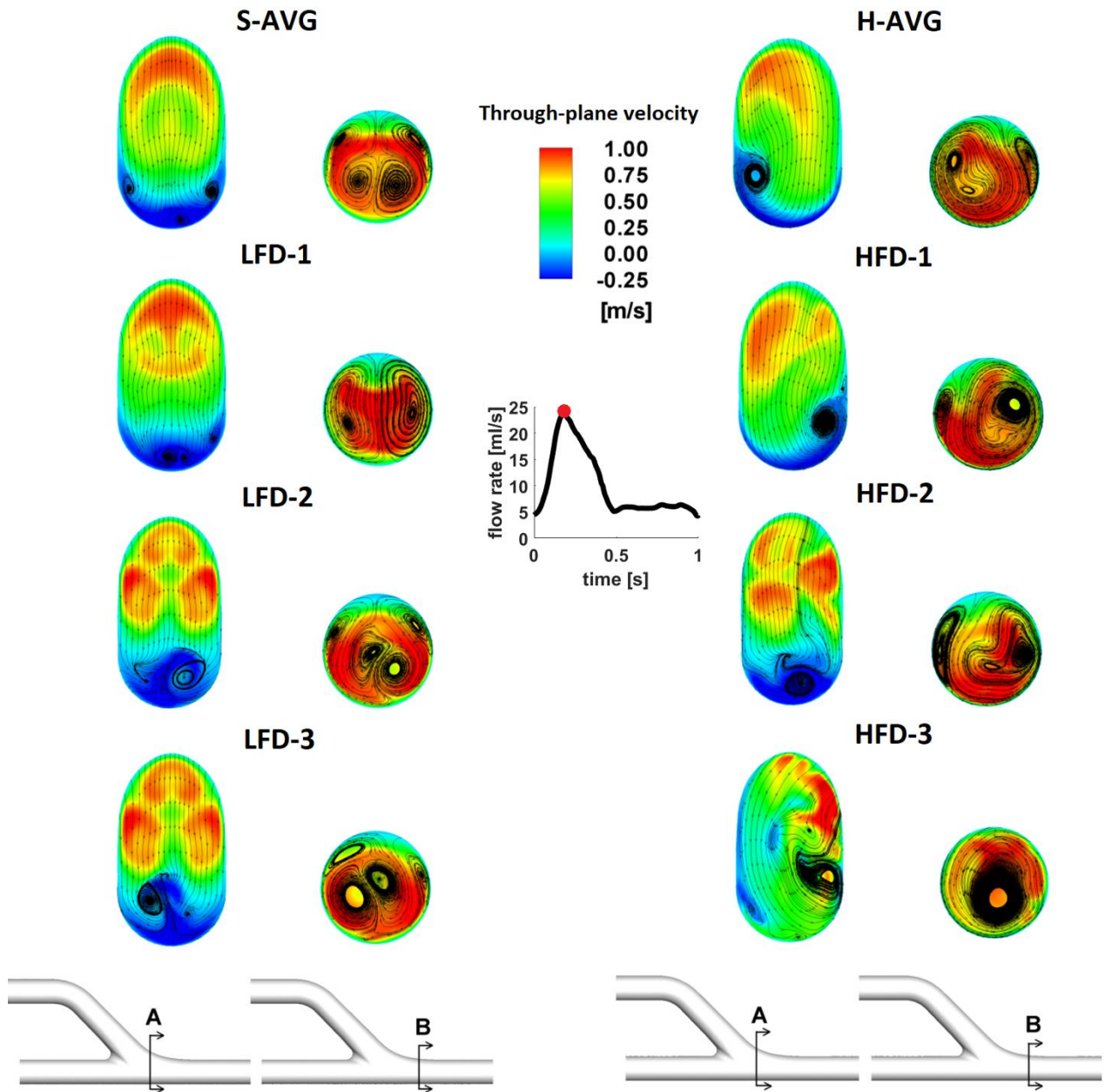
**Figure 4.** Percentage difference in mean values of WSS-based descriptors (TAWSS, OSI, and RRT) at the ROI with respect to: A) S-AVG model; B) H-AVG model. Beneficial effects are green-coloured; detrimental effects are orange-coloured.



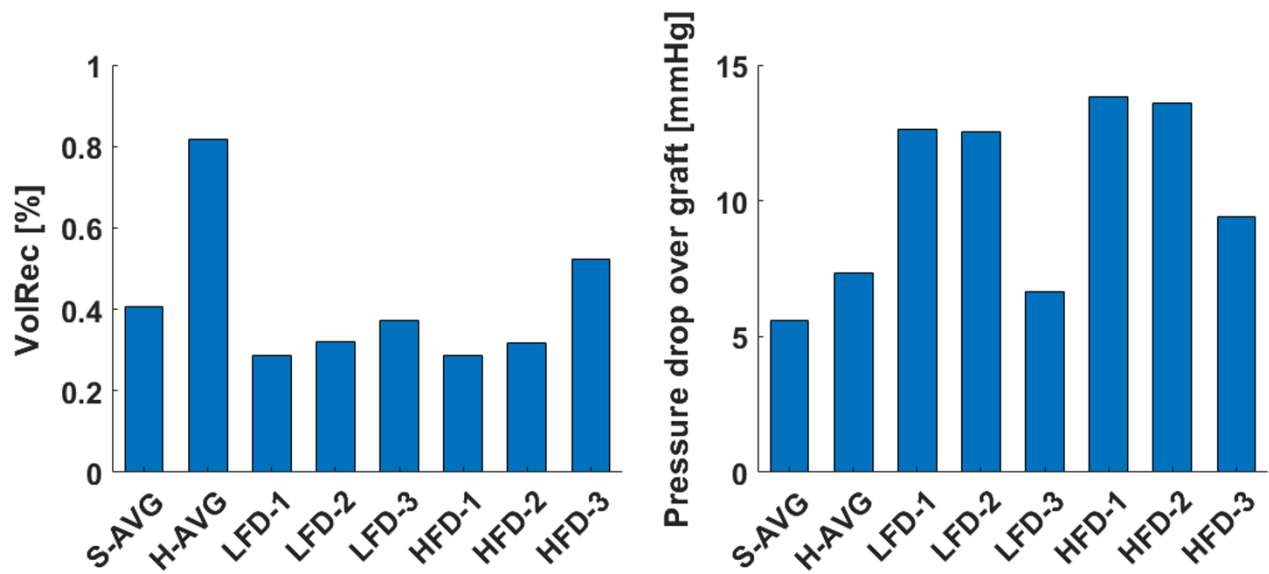
**Figure 5.** Distributions for surface area exposed to 'disturbed shear' at the ROI. Red colour delimits the surface area at the ROI exposed to TAWSS values lower (higher for OSI and RRT) than the defined thresholds, defining TAWSS20, OSI80 and RRT80.



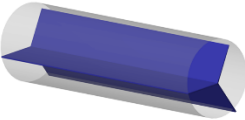
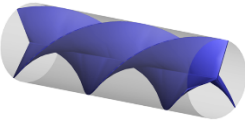
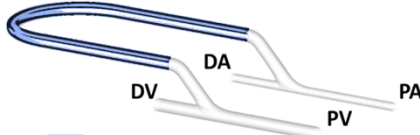
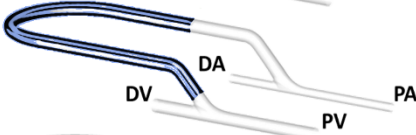
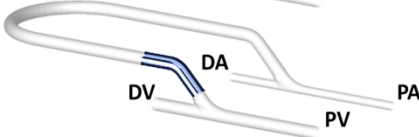
**Figure 6.** Visualization of LNH cycle-average isosurfaces ( $LNH=\pm 0.4$ ) for the eight different models of AVGs: blue and red colours identify left-handed and right-handed helical flow rotation, respectively.



**Figure 7.** Colour maps of through-plane velocity, shown with streamlines of in-plane velocity at peak systole for two different cross section at the venous segment of the investigated AVG models. Cross section A is located at the venous anastomosis; cross section B 10 mm downstream of the venous anastomosis. The volume flow rate waveform applied as inflow condition was also reported, with a red marker indicating peak systole.



**Figure 8.** Normalized volume of recirculating flow (left) and pressure drop (right) at the graft segment of each model.

	IH risk	Thrombus risk	Pressure drop
<b>FD shape</b>			
	↑↑	≈	↑
	↓↓	≈	↑↑
	IH risk	Thrombus risk	Pressure drop
<b>FD positioning</b>			
	≈	↓	↑↑
	≈	↓	↑↑
	↓↓	≈	↑
≈ almost equal    ↓ or ↑ moderate    ↓↓ or ↑↑ more pronounced			

**Figure 9.** Qualitative scheme summarizing the results in terms of potential hemodynamic-related IH risk, potential thrombosis risk, and pressure drop over the graft as a consequence of different FD shapes and positions. Model S-AVG is taken as reference.